Article

Cell Reports

Myosin VI Contains a Compact Structural Motif that Binds to Ubiquitin Chains

Graphical Abstract

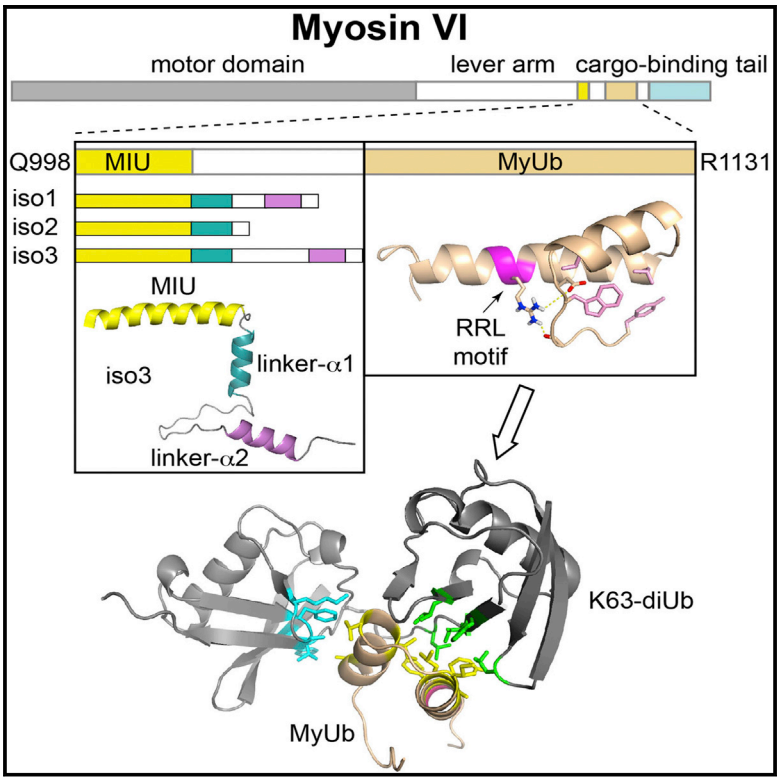

Highlights

- Myosin VI contains a compact structural motif that binds ubiquitin chains
- MyUb nestles between ubiquitins of K63-linked chains
- Optineurin interaction requires an expanded MyUb and capacity to bind ubiquitin
- An isoform-specific helix restricts MyUb binding to ubiquitin chains

Authors

Fahu He, Hans-Peter Wollscheid, Urszula Nowicka, ..., Elisa Magistrati, Simona Polo, Kylie J. Walters

Correspondence

simona.polo@ifom.eu (S.P.), kylie.walters@nih.gov (K.J.W.)

In Brief

He et al. identify a UBD in myosin VI (MyUb) and solve its structure in the free and K63-linked diubiquitin-bound state. An isoform-specific helix restricts MyUb binding to ubiquitin. Myosin VI binding to the autophagy adaptor optineurin requires an expanded MyUb structure as well as a functional ubiquitin-binding surface.

Accession Numbers

2N0Z
2N10
2N11
2N13

He et al., 2016, Cell Reports *14*, 2683–2694
March 22, 2016
http://dx.doi.org/10.1016/j.celrep.2016.01.079

CellPress

Cell Reports
Article

Myosin VI Contains a Compact Structural Motif that Binds to Ubiquitin Chains

Fahu He,[1,5] Hans-Peter Wollscheid,[2,5,6] Urszula Nowicka,[1] Matteo Biancospino,[2] Eleonora Valentini,[2] Aaron Ehlinger,[3,7] Filippo Acconcia,[2,8] Elisa Magistrati,[2] Simona Polo,[2,4,*] and Kylie J. Walters[1,*]
[1]Protein Processing Section, Structural Biophysics Laboratory, Center for Cancer Research, National Cancer Institute, Frederick, MD 21702, USA
[2]IFOM, Fondazione Istituto FIRC di Oncologia Molecolare, Via Adamello 16, 20139 Milano, Italy
[3]Department of Biochemistry, Molecular Biology and Biophysics, University of Minnesota, Minneapolis, MN 55455, USA
[4]DIPO, Dipartimento di Oncologia ed Emato-oncologia, Università degli Studi di Milano, Via di Rudinì 8, 20122 Milan, Italy
[5]Co-first author
[6]Present address: Institute of Molecular Biology, 55128 Mainz, Germany
[7]Present address: Center for Structural Biology, Vanderbilt University, Nashville, TN 37240, USA
[8]Present address: University of Rome "ROMA TRE," 00154 Rome, Italy
*Correspondence: simona.polo@ifom.eu (S.P.), kylie.walters@nih.gov (K.J.W.)
http://dx.doi.org/10.1016/j.celrep.2016.01.079

SUMMARY

Myosin VI is critical for cargo trafficking and sorting during early endocytosis and autophagosome maturation, and abnormalities in these processes are linked to cancers, neurodegeneration, deafness, and hypertropic cardiomyopathy. We identify a structured domain in myosin VI, myosin VI ubiquitin-binding domain (MyUb), that binds to ubiquitin chains, especially those linked via K63, K11, and K29. Herein, we solve the solution structure of MyUb and MyUb:K63-linked diubiquitin. MyUb folds as a compact helix-turn-helix-like motif and nestles between the ubiquitins of K63-linked diubiquitin, interacting with distinct surfaces of each. A nine-amino-acid extension at the C-terminal helix (Helix2) of MyUb is required for myosin VI interaction with endocytic and autophagic adaptors. Structure-guided mutations revealed that a functional MyUb is necessary for optineurin interaction. In addition, we found that an isoform-specific helix restricts MyUb binding to ubiquitin chains. This work provides fundamental insights into myosin VI interaction with ubiquitinated cargo and functional adaptors.

INTRODUCTION

Myosins are a superfamily of quintessential molecular motors that power movements on actin filaments by converting ATP hydrolysis to mechanical energy and force. A highly conserved N-terminal motor domain undergoes conformational changes during the ATPase cycle that modulate actin affinity (Geeves and Holmes, 1999). These motions are amplified into the myosin powerstroke by a variable calmodulin-binding lever arm causing nanometer-scale movement (Spudich and Sivaramakrishnan, 2010). With the exception of myosin VI, movement is toward the barbed (plus) end of actin filaments (Wells et al., 1999). Myosin VI contains an additional calmodulin-binding insertion that redirects the effective lever arm toward the pointed (minus) end of actin filaments (Ménétrey et al., 2005). The C-terminal tail region is divergent among myosins and confers specificity for cargo and distinct interactions that define subcellular localization and specialized functions.

Humans express ~40 known or predicted myosins (Berg et al., 2001) that participate in diverse activities, including conventional skeletal myosin IIs for muscle contraction and unconventional myosins that function in intracellular trafficking, cell division and motility, actin cytoskeletal organization, and cell signaling (Sellers, 2000). Myosin malfunction has been implicated in hypertrophic cardiomyopathy (Mohiddin et al., 2004), Usher syndrome (Hasson et al., 1995; Weil et al., 1995), deafness (Avraham et al., 1995; Gibson et al., 1995), Griscelli syndrome (Kumar et al., 2001; Takagishi and Murata, 2006), and cancer (Dunn et al., 2006; Yoshida et al., 2004), thus prompting the development of small-molecule myosin inhibitors (Bond et al., 2013).

The myosin VI cargo-binding tail (Figure 1A) interacts with multiple adaptor proteins, including regulators of clathrin-mediated endocytosis and autophagy (Tumbarello et al., 2013). Some of these ligands require a myosin VI Arg-Arg-Leu (RRL) motif (Figure 1C), including nuclear dot protein 52 (NDP52) (Morriswood et al., 2007), Traf6-binding protein (T6BP) (Morriswood et al., 2007), optineurin (Sahlender et al., 2005), and GAIP-interacting protein C terminus (GIPC) (Bunn et al., 1999; Spudich et al., 2007). Others engage a Trp-Trp-Tyr (WWY) triplet present in the cargo-binding domain (CBD; Figure 1A), including Tom1/Tom1L2 (Finan et al., 2011; Tumbarello et al., 2012), Dab2 (Inoue et al., 2002; Morris et al., 2002; Spudich et al., 2007), and lemur tyrosine kinase-2 (LMK2) (Chibalina et al., 2007).

We previously reported the existence of a motif interacting with ubiquitin (MIU) domain C-terminal to the myosin VI coiled-coil region (Penengo et al., 2006) (Figure 1A, yellow). In this article, we identify a second ubiquitin-binding domain (UBD) in

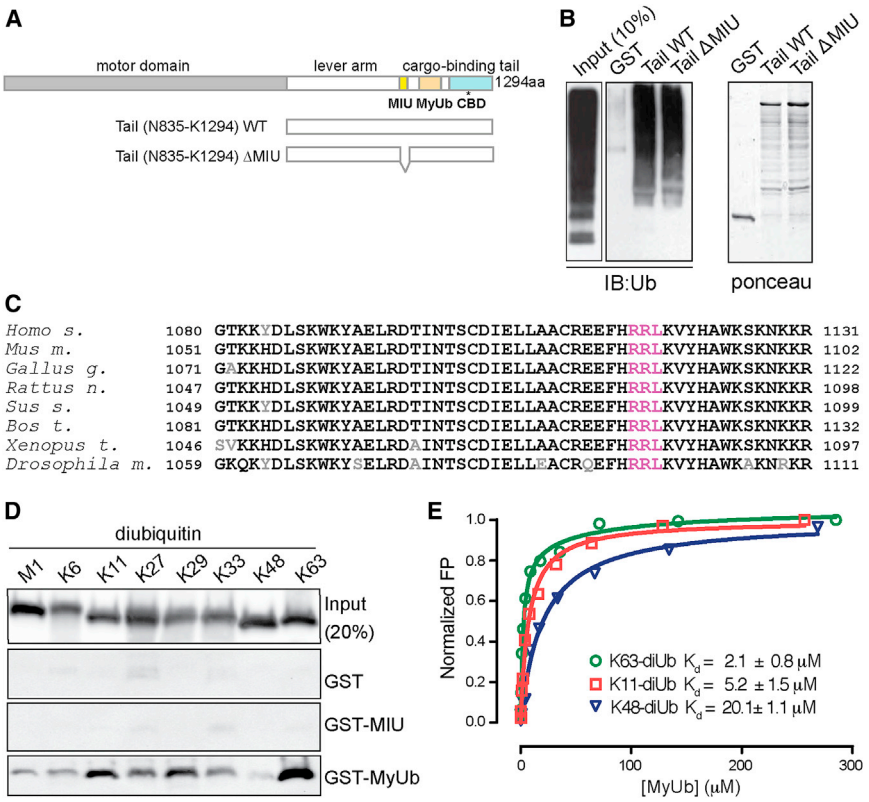

Figure 1. Identification and Characterization of the MyUb Domain

(A) Domain architecture of myosin VI highlighting the motor domain (gray), lever arm (white), MIU (yellow), MyUb (beige), and cargo-binding domain (CBD; light blue). The WWY motif is in the CBD and noted with an asterisk. aa, amino acid. Depicted below are the tail constructs used for the experiment described in (B).

(B) GST-tagged myosin VI tail (N835–K1294) wild-type and mutant carrying an internal deletion of the MIU domain (S997–I1024) were used to pull down polyubiquitinated proteins from HEK293T cellular lysates. Immunoblotting (IB) as indicated. Right: ponceau showing equal loading of the GST proteins.

(C) Sequence alignment of MyUb from *Homo sapiens*, *Mus musculus*, *Gallus gallus*, *Rattus vorvegicus*, *Sus scrofa*, *Bos Taurus*, *Xenopus tropicalis*, and *Drosophila melanogaster* with conserved and non-conserved amino acids in black and gray, respectively. The RRL motif is highlighted in magenta.

(D) GST pull-down assay with indicated myosin VI constructs or GST as a control. GST-fusion proteins were incubated with purchased diubiquitins linked by M1, K6, K11, K27, K29, K33, K48, or K63 (Boston Biochem) and analyzed by immunoblotting with anti-ubiquitin antibody.

(E) Fluorescence polarization (FP) assays to determine MyUb binding affinities for K63-, K48-, and K11-linked diubiquitin. Results are representative of at least three independent experiments. Dissociation constants with their respective SD are reported. See also Figure S1.

myosin VI, which we name MyUb (myosin VI ubiquitin-binding domain), that contains the RRL motif. We use nuclear magnetic resonance (NMR) spectroscopy to find that MyUb adopts a compact protein fold that is required for ubiquitin binding and disrupted by amino acid substitutions in the RRL motif. We evaluate MyUb in the context of myosin VI binding to the autophagy adaptor optineurin and the distinct myosin VI isoforms expressed in humans.

RESULTS

Identification of a Ubiquitin-Binding Domain in Myosin VI: The MyUb

In Rabex-5, the MIU domain binds to ubiquitinated epidermal growth factor receptor and promotes coupled monoubiquitination (Penengo et al., 2006). To obtain insight into the function of the MIU (Q998–S1025) in the context of myosin VI (Figure 1A), we analyzed the myosin VI tail spanning N835–K1294, which recapitulates myosin VI interaction and localization (Buss et al., 2001). Surprisingly, deletion of the MIU domain (S997–I1024) did not abrogate myosin VI tail binding to ubiquitinated species from cellular lysates (Figure 1B). Deletion analysis led to the identification of a second UBD C-terminal to the identified MIU (Figure 1A), which we narrowed down to a 43-amino-acid fragment (G1080–H1122; Figures S1A–S1C). This region is highly conserved in myosin VI from various species (Figure 1C) and appears to be unique to myosin VI, as bioinformatics analysis was unable to detect its presence in other genes (Kay Hoffman, personal communication). Since this region lacks sequence similarity with any previously described UBD, we henceforth refer to it as MyUb.

We used diubiquitin molecules made with the eight possible linkages (M1, K6, K11, K27, K29, K33, K48, and K63) to test whether MyUb or MIU exhibit preference for a specific chain type. glutathione S-transferase (GST)-MIU binding to diubiquitin was barely detectable by this method (Figure 1D); on the contrary, GST-MyUb bound robustly to ubiquitin chains, with preference for K63-, K11-, and K29-linked diubiquitin (Figure 1D). Weak interaction was detected with K48-linked diubiquitin (Figure 1D), a linkage type associated with proteasomal degradation (Ehlinger and Walters, 2013). This difference in affinity was confirmed by fluorescence polarization (FP) assays. MyUb bound to K11-, K48-, and K63-linked diubiquitin with low micromolar affinity, with the K63- and K11-linked diubiquitin exhibiting 10- and 4-fold greater affinity compared to K48-linked diubiquitin, respectively (Figure 1E).

Solution Structure of MyUb Reveals a Compact Fold that Is Critical for Binding to Ubiquitin and Adaptors for Endocytosis and Autophagy

We used NMR techniques (described in Experimental Procedures) to solve the MyUb (G1080–H1122) structure. The 20 lowest-energy structures calculated from 100 extended starting ones converged to fit recorded NMR data (Table S1), with a backbone root mean square deviation (rmsd) of 0.20 Å (Figure S2A). From these data, we concluded that MyUb adopts a

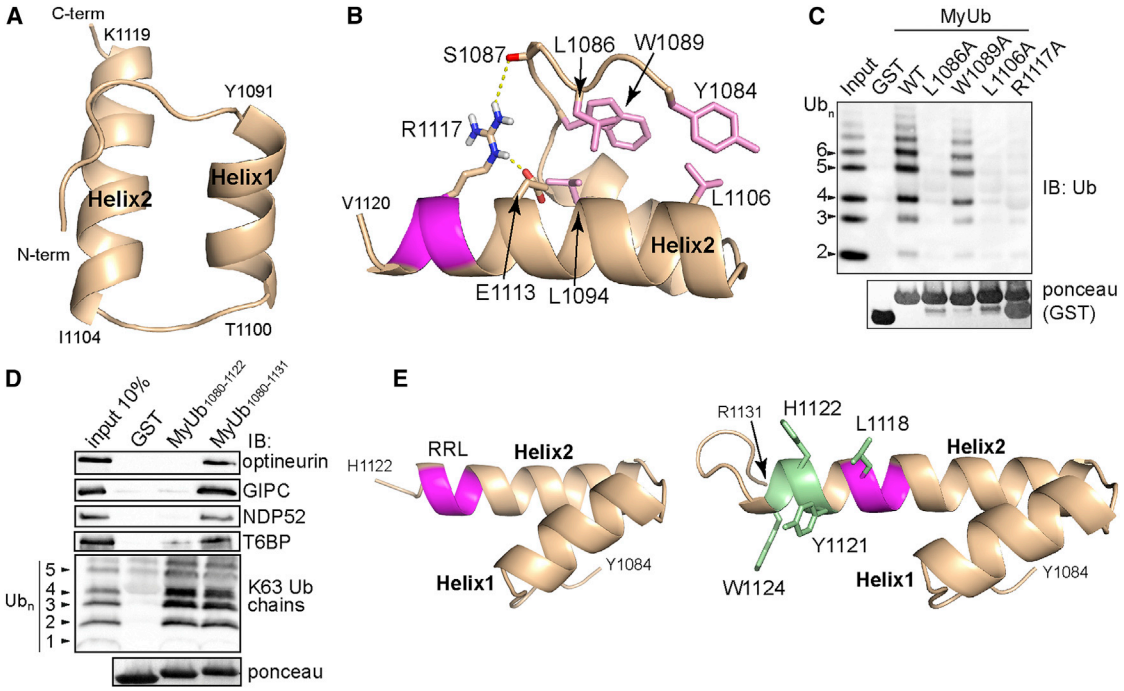

Figure 2. Myosin VI Contains a Compact Ubiquitin-Binding Domain

(A and B) Ribbon representation of MyUb (G1080–H1122) highlighting the helix boundaries and the interactions that stabilize the fold, including hydrogen bonds from R1117 to S1087 and E1113 (dashed yellow lines) and van der Waals interactions engaging Y1084, L1086, W1089, L1094, and L1106 (pink).

(C) GST pull-down assay performed with GST-MyUb (G1080–R1131) wild-type (WT) or amino-acid-substituted protein as indicated. GST fusion proteins were incubated for 2 hr at 4°C with K63-linked polyubiquitin$_{1-7}$ and analyzed by immunoblotting (IB) with anti-ubiquitin antibody. Ponceau staining shows comparable loading of GST-tagged proteins (bottom). GST was used as a negative control.

(D) GST-MyUb (G1080–H1122), GST-MyUb (G1080–R1131), or GST (as a negative control) were incubated with synthetic K63-linked polyubiquitin$_{1-7}$ or cellular lysates from HEK293T cells transfected with GFP-optineurin, FLAG-T6BP, His-GIPC, or FLAG-NDP52. Immunoblotting (IB) was performed using the specific anti-TAG antibodies. Ponceau staining shows comparable loading of GST-tagged proteins (bottom).

(E) Ribbon representations of MyUb (G1080–H1122) (left) and MyUb (G1080–R1131) with extended hydrophobic surface highlighted in green formed by addition of A1123–R1131 (right) were shown. The RRL motif is colored magenta.

See also Figure S2.

compact helix-turn-helix-like fold with two helices spanning Y1091 to T1100 (Helix1) and I1104 to K1119 (Helix2) (Figure 2A). Importantly, the structural fold is stabilized by numerous interactions with an N-terminal region (Figure 2B). Y1084 and L1086 from the N-terminal region pack against hydrophobic amino acids (L1094 and L1106) from Helix2, while W1089 is partially buried by L1094 and L1086 (Figure 2B, pink). Alanine substitution of L1086 or L1106 causes misfolding of the MyUb domain (Figures S2B and S2C) and significantly decreased binding to K63-linked ubiquitin chains (Figure 2C). A W1089A mutation was instead tolerated, as it did not fully disrupt the MyUb structure (Figure S2D) and did not prevent MyUb binding to K63-linked diubiquitin (Figures 2C and S2E). Changing the temperature and salt conditions did not alter MyUb structure (Figures S2F–S2H) or interaction with K63-linked diubiquitin (Figure S2I).

Several myosin VI adaptor proteins, namely optineurin, GIPC, T6BP, and NDP52, were shown to require an intact ^{1116}RRL^{1118} motif for interaction with myosin VI (Bunn et al., 1999; Morriswood et al., 2007; Sahlender et al., 2005; Spudich et al., 2007). In particular, amino acid substitution of this motif with the alanine triple AAA was reported to abolish myosin VI interaction with these autophagy adaptor proteins (Morriswood et al., 2007). The RRL motif resides in Helix2 where R1117 forms hydrogen bonds to S1087 and E1113 (Figure 2B), suggesting that it is critical for MyUb (G1080–H1122) structural integrity. As expected, replacement of R1117 with alanine resulted in misfolding, as measured by a 2D NMR experiment (Figure S2J, red compared to black) and abolished interaction with ubiquitin (Figure 2C).

This result prompted us to re-examine the interaction of myosin VI with previously characterized autophagy adaptor proteins using various RRL-containing fragments. The minimal binding region was found to be a MyUb construct spanning G1080–R1131 (Figure 2D). The shorter construct spanning G1080–H1122 was unable to bind optineurin, GIPC, T6BP, and NDP52, even though it was competent for binding to ubiquitin (Figures 2D and S2K) and adopted a stable protein fold (Figure 2A). Thus, the interaction surface between myosin VI and its known partners extends beyond the previously identified ^{1116}RRL^{1118} motif toward the C-terminal part of Helix2 of the MyUb domain. We next used NMR to solve the structure of this longer construct (Figure S2L; Table S1). The backbone rmsd of the extended MyUb (G1080–R1131) to MyUb (G1080–H1122) was 0.46 Å for the overlapping region. Helix 2 was extended, however, by six amino acids forming an additional

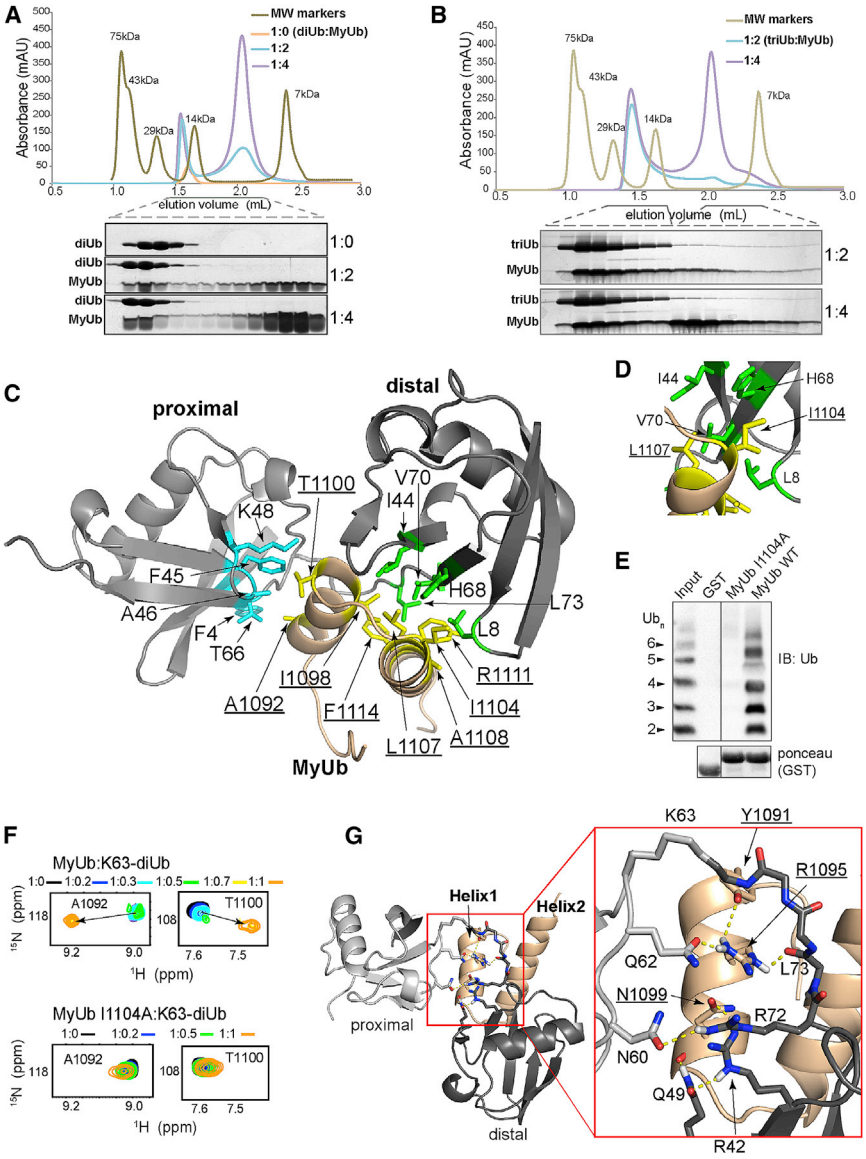

Figure 3. MyUb Nestles between the Moieties of K63-Linked Diubiquitin

(A and B) Stoichiometry of the complex formed by MyUb and K63-linked (A) diubiquitin or (B) triubiquitin, as indicated. 100 μM purified K63-linked diubiquitin or K63-linked triubiquitin was incubated (1 hr, 20°C) with either 200 or 400 μM MyUb, followed by fractionation on a Superdex75 column. Selected fractions were separated by SDS-PAGE gel and stained with Coomassie.

(C) Ribbon diagram of MyUb (G1080–H1122):K63-linked diubiquitin with MyUb (beige) nestled between the proximal ubiquitin (light gray) and distal ubiquitin (dark gray) with interactions to a I44-centered surface on distal ubiquitin (green) and a F45-centered surface of proximal ubiquitin (blue). Interacting MyUb amino acids are displayed in yellow. Labels for MyUb amino acids are underlined.

(D) Expanded view of (C) showing critical interactions of I1104 from MyUb with L8 and H68 of the distal K63-linked diubiquitin.

(E) GST pull-down assay performed with GST-MyUb (G1080–R1131) wild-type (WT) or I1104A. GST fusion proteins were incubated for 2 hr at 4°C with K63-linked polyubiquitin$_{1-7}$ and analyzed by immunoblotting (IB) with anti-ubiquitin antibody. Ponceau staining shows comparable loading of GST-tagged proteins (bottom). GST was used as a negative control.

(F) Selected regions that include A1092 and T1100 signals from ^{1}H-^{15}N HSQC spectra acquired on ^{15}N-labeled MyUb wild-type (top) or MyUb I1104A (bottom) with K63-linked diubiquitin at the indicated molar ratio. Arrows point to new peak positions caused by addition of diubiquitin. All spectra were recorded at 850 MHz on MyUb sample concentrations of 0.1 mM.

(G) Ribbon diagrams of the MyUb:K63-linked diubiquitin complex showing the opposite surface compared to (C), rotated 145 degrees along the x axis, to highlight hydrogen bond (yellow dashed line) interactions involving MyUb and K63-linked diubiquitin. An expanded region (boxed in red) is displayed to the right.

See also Figure S3.

1.5 helical turns, with an expanded hydrophobic surface contributed by Y1121, H1122, and W1124 (Figure 2E, right). We speculate that this extended hydrophobic surface is involved in myosin VI binding to autophagy adaptor proteins.

MyUb Nestles between Ubiquitins of K63-Linked Diubiquitin

The MyUb bound well to K11-, K29, and K63-linked ubiquitin chains (Figure 1D). We therefore used K63-linked diubiquitin as a model to dissect the molecular mechanism of MyUb binding to ubiquitin chains. Initially, we determined the binding stoichiometry of the MyUb:K63-linked ubiquitin chain complex by using size exclusion chromatography. 2- or 4-fold molar excess MyUb incubated with 100 μM diubiquitin or triubiquitin was loaded on a size exclusion column (Figures 3A and 3B). At 2-fold molar excess, MyUb and K63-linked diubiquitin co-eluted at the expected molecular weight for a 1:1 complex with the excess MyUb eluting separately (Figure 3A, blue). By contrast, very little MyUb eluted separately from K63-linked triubiquitin (Figure 3B, blue), and the presence of free MyUb in the mixture with triubiquitin increased significantly when MyUb was at 4-fold molar excess (Figure 3B, purple). Altogether, these data indicate a 1:1 stoichiometry for the MyUb:diubiquitin complex and a 2:1 stoichiometry for the MyUb:triubiquitin complex.

To explore the molecular basis of MyUb binding to ubiquitin, we used NMR to solve the structure of MyUb (G1080–H1122) in complex with K63-linked diubiquitin. The MyUb structure was unchanged upon ubiquitin binding, as demonstrated by an almost identical interaction network for free and K63-linked diubiquitin-bound MyUb (Figure S3A). We isotopically labeled either the proximal (defined by a free G76 that can be in principle conjugated to a substrate protein) or the distal ubiquitin of

K63-linked diubiquitin and used ^{13}C half-filtered nuclear Overhauser effect spectroscopy (NOESY) experiments to detect interactions between MyUb and each ubiquitin (Figures S3B–S3D). We were able to assign 59 intermolecular interactions between MyUb and the proximal ubiquitin and 47 intermolecular interactions between MyUb and the distal ubiquitin; these were used to solve the structure of the MyUb:K63-linked diubiquitin complex (Figures S3E and S3F; Table S1). We found that MyUb nestles between the two ubiquitins, making extensive contacts to both ubiquitin moieties (Figure 3C).

On the distal ubiquitin, an exposed MyUb hydrophobic surface formed by the two helices contacts the classic hydrophobic patch centered on I44 (Liu and Walters, 2010) (Figure 3C, green). This contact surface includes I1098 from Helix1 and I1104, L1107, A1108, R1111, and F1114 from Helix2 (Figure 3C, yellow). In particular, I1104 forms critical interactions with L8 and H68 of distal ubiquitin (Figure 3D). Its replacement with alanine does not affect the overall MyUb fold (Figure S3G) but abolishes binding to K63-linked diubiquitin, as shown in a pull-down experiment (Figure 3E) and by NMR titration experiments (Figure 3F). In the slow exchange regime on the NMR timescale (Walters et al., 2001), amino acids A1092 and T1100 shift to a new position upon K63-linked diubiquitin addition (Figure 3F, top panels). This effect is lost in the MyUb I1104A mutant (Figure 3F, bottom). These data were confirmed by FP analysis, which demonstrated a K_d >400 μM for the I1104A mutant (Figure S3H).

On the proximal ubiquitin, aforementioned A1092 and T1100 from Helix1 of MyUb contact a surface formed by F4, F45, A46, K48, and T66 (Figure 3C, blue). Likely, the involvement of K48 at this location explains the relatively poor affinity of the MyUb for this chain type (Figures 1D and 1E). Some nuclear Overhauser effects (NOEs) were assigned to the L8-I44-V70 hydrophobic patch of the proximal ubiquitin, indicating that MyUb can form a lower affinity interaction with this region (Figures S3C and S3F, orange, and S3I). However, binding to this second, low-affinity site was not retained in the size exclusion chromatography experiment (Figure 3A), indicating that this interaction is weak and possibly not present in the context of the full-length protein.

MyUb interaction with K63-linked diubiquitin is stabilized by electrostatic contacts that surround the ubiquitin isopeptide region (Figure 3G). MyUb R1095 forms hydrogen bonds with distal ubiquitin L73 and proximal ubiquitin Q62. Distal ubiquitin R42 and Q49 are spatially close to MyUb N1099 and form hydrogen bonds with its side chain and backbone, respectively.

We also explored how MyUb binds to K11-linked diubiquitin taking advantage of K11-linked diubiquitin in which either the proximal or distal ubiquitin was ^{13}C and ^{15}N labeled. We found in a ^{13}C half-filtered NOESY experiment that L8 and I44 from the proximal K11-linked ubiquitin formed similar contacts to MyUb as was observed for the distal K63-linked ubiquitin component (Figure 4A). For example, L8 and I44 from the proximal ubiquitin of K11-linked diubiquitin were similarly shown to directly interact with I1104 from MyUb (Figure 4A). No such intermolecular NOE interactions were observed for L8 or I44 from the distal ubiquitin of K11-linked diubiquitin (data not shown). Furthermore, the I44 and A46 amide signals from the proximal, but not distal, ubiquitin demonstrated significant shifting following addition of equimolar MyUb (Figure 4B, orange versus black). Taken together, our data suggest that MyUb prefers the hydrophobic patch of proximal ubiquitin to distal ubiquitin in the context of K11-linked diubiquitin and that the proximal ubiquitin hydrophobic patch of K11-linked diubiquitin binds to MyUb in a similar mode as that observed for distal ubiquitin of K63-linked diubiquitin (Figures 4C and 3C). Further studies are needed to solve the structure of this MyUb complex, but we concluded that MyUb binds to K11-linked chains in a distinct manner that involves contacts between MyUb I1104 and the L8 and I44 methyl groups (Figures 4A and 4C).

The Ubiquitin-Binding Ability of MyUb Contributes to Optineurin Interaction

Optineurin is a well-characterized myosin VI interactor. Previous work has suggested a direct interaction mediated by the RRL motif in myosin VI and the UBDs of optineurin (Sahlender et al., 2005; Shen et al., 2015). Our results suggest that ubiquitin may be part of the myosin VI interaction with this adaptor protein.

To investigate this issue, we first analyzed whether optineurin undergoes ubiquitination. HEK293T cells were transfected with GFP-optineurin and HA-ubiquitin and the cell lysate subjected to immunoprecipitation using anti-HA antibody. As visible in Figure 5A, optineurin is poly- or multi-ubiquitinated under these conditions. The lysate was next used for a pull-down assay in which we compared MyUb wild-type (WT) with the ubiquitin-binding-impaired I1104A mutant (Figure 3E). WT MyUb bound strongly to the ubiquitinated form of optineurin, while the I1104A mutant retained only a basal interaction with this autophagic adaptor (Figure 5B). Notably, the I1104A mutant also showed a clear impairment for ubiquitin binding in vivo where ubiquitinated proteins were robustly immunoprecipitated with the WT protein (Figure 5B). Similar results were obtained incubating immunoprecipitated GFP-optineurin with GST proteins eluted from the beads (Figure 5C). Altogether, these results indicate that the ubiquitin-binding surface of the MyUb participates in binding to this RRL interactor, either by direct binding or by binding to ubiquitin that is conjugated to optineurin.

MIU Exists within a Long α Helix that Kinks into a Shorter Linker Helix

We have previously identified an MIU domain that is C-terminal to the myosin VI coiled-coil region (Penengo et al., 2006) (Figure 6A). We tested whether we could detect binding between a peptide that encompasses the myosin VI MIU (spanning Q998–S1025) and ubiquitin by NMR. Unlabeled ubiquitin was added to ^{15}N-labeled MIU and the effects recorded (Figure 6B). Shifting and disappearance of MIU signals was observed with ubiquitin addition (Figures 6B and S4A), including signals from A1013 and L1014, which were predicted to be at the center of the MIU ubiquitin-binding surface (Penengo et al., 2006). By contrast, unlabeled MyUb did not affect NMR spectra recorded on ^{15}N MIU (Figure S4B), indicating that these two structural elements do not interact. In support of this finding, the MIU is not significantly different in spectra recorded on the MIU by itself (Q998–S1025) compared to in the context of the MIU-MyUb region (Q998–R1131; Figure S4C), similarly demonstrating that it does not interact with these other regions of the protein.

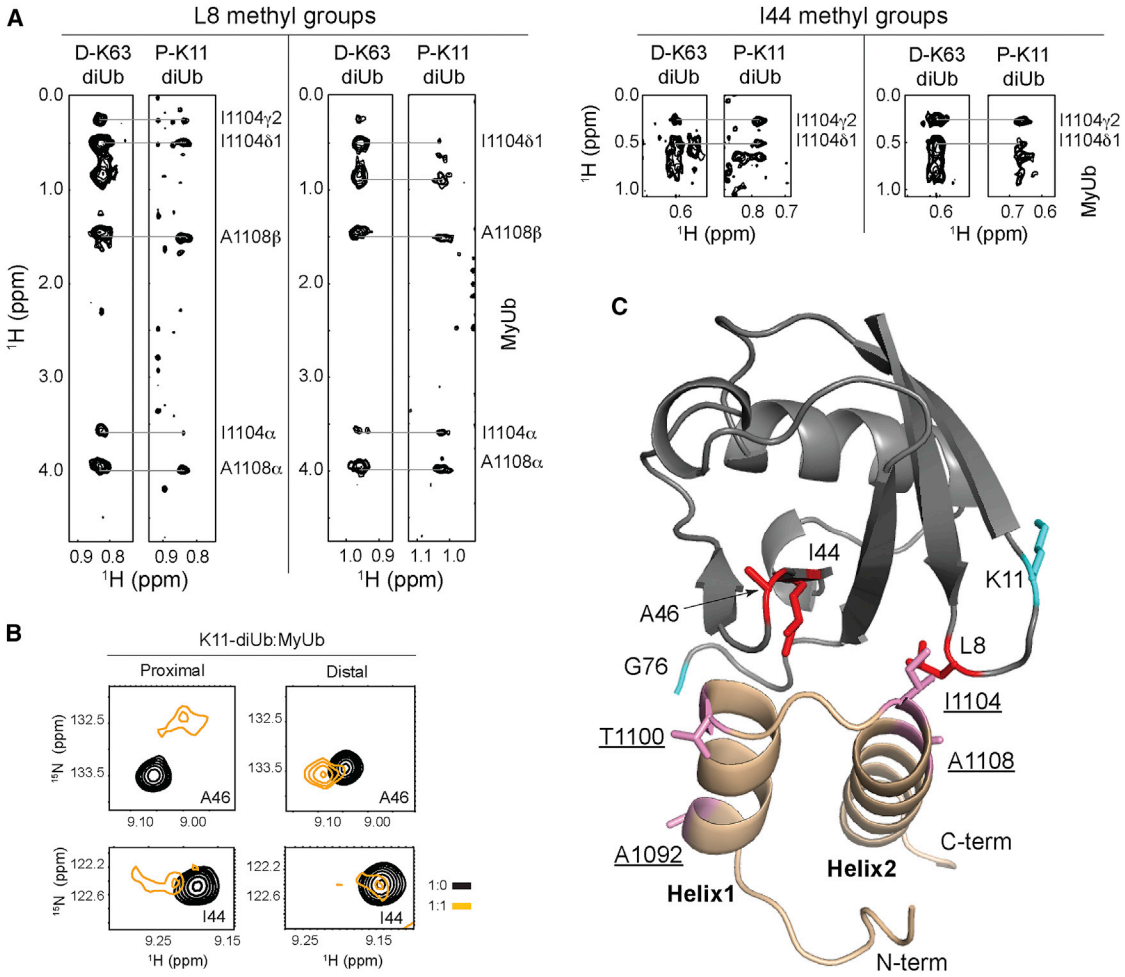

Figure 4. MyUb Binds to K11-Linked Diubiquitin through the Hydrophobic Patch of the Proximal Ubiquitin Moiety

(A) Selected regions showing methyl groups from L8 and I44 from a 3D ^{13}C half-filtered NOESY experiment acquired on ~0.5 mM unlabeled MyUb (G1080–H1122) mixed with equimolar K63- (left) or K11-linked (right) diubiquitin with the proximal or distal ubiquitin moiety ^{15}N and ^{13}C labeled, respectively. NOEs assigned uniquely to MyUb atoms are labeled. D-K63, K63-linked diubiquitin with the distal moiety ^{15}N and ^{13}C labeled; P-K11, K11-linked diubiquitin with the proximal moiety ^{15}N and ^{13}C labeled.

(B) Selected regions that include A46 and I44 amide signals from ^{1}H-^{15}N HSQC spectra acquired on ^{13}C, ^{15}N-labeled proximal (left) or distal (right) K11-linked diubiquitin (black) and with equimolar unlabeled MyUb (orange).

(C) Model structure of MyUb bound to a single ubiquitin based on Figure 3C, illustrating the amino acids involved in complex formation as revealed in (A) and (B).

Myosin VI is generated by alternatively spliced isoforms, which are differentially expressed in tissues and cell lines, and associated with specific subcellular compartments (Au et al., 2007; Buss et al., 2001; Tomatis et al., 2013). These isoforms differ by insertions in the cargo-binding tail. Notably, the large insert (LI) (Buss et al., 2001) separates the two myosin VI UBDs, the MIU (Penengo et al., 2006) and the MyUb (Figure 6A). We first tested whether the presence of the LI variable exons (as expressed in isoform1 [iso1] and isoform3 [iso3]) has an impact on MyUb binding to ubiquitin by using pull-down assays. Compared to isoform2 (iso2) MIU-MyUb, iso1/3 MIU-MyUb exhibited reduced overall binding to ubiquitinated proteins from cellular lysates (Figure 6C). Moreover, the iso2 MIU-MyUb fragment that lacks the LI bound short K63-linked ubiquitin chains more robustly (Figure 6D). FP analysis with K63-linked diubiquitin corroborated these data, indicating iso1 and iso3 MIU-MyUb to have a 4- to 5-fold reduction in ubiquitin-binding strength compared to iso2 MIU-MyUb (Figures 6E and S4D–S4F). Thus, the presence of the LI led to reduced affinity of the myosin VI ubiquitin-binding region for K63-linked ubiquitin chains.

We also tested whether the MIU-MyUb region from iso1/3 and iso2 exhibit differences in affinity for K11- and K48-linked diubiquitin by using FP. We similarly found higher affinity for iso2 compared to iso1/3, with ~5- and ~3-fold greater affinity for K11- and K48-linked chains, respectively (Figure 6E). Interestingly, binding to K63- and K48-linked diubiquitin is similar between MyUb and iso2, whereas K11-linked diubiquitin binds with a greater affinity to iso2 compared to MyUb (Figures 6E and S4E), indicating a possible contribution of the MIU domain in myosin VI for K11-linked ubiquitin chains. To test the

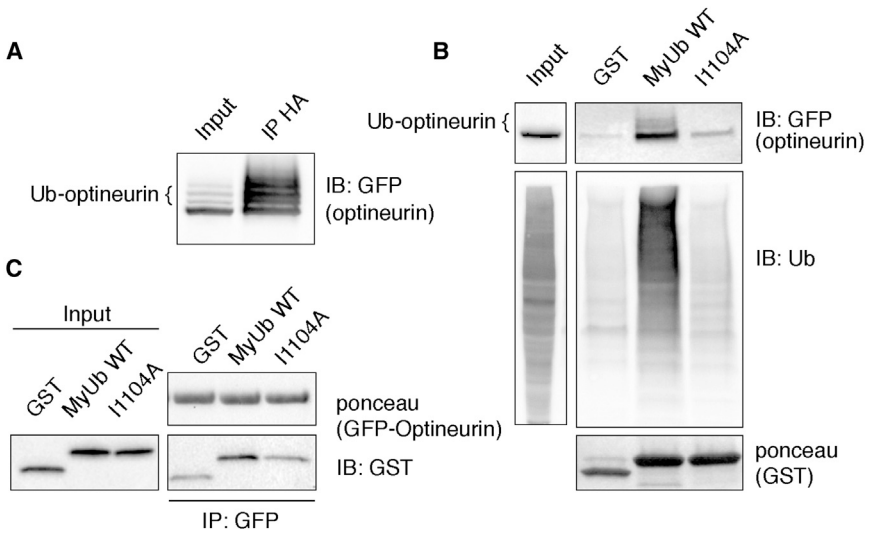

Figure 5. Ubiquitin Binding by MyUb Contributes to Myosin VI/Optineurin Interaction

(A) Lysate from HEK293T cells expressing GFP-optineurin and HA-ubiquitin was immunoprecipitated and immunoblotted as indicated.

(B) 2 μM of the indicated GST-fusion proteins was incubated with the same cellular lysate (2 mg) shown in (A). Immunoblotting was performed using anti-GFP or anti-ubiquitin antibodies. Ponceau staining shows comparable loading of GST-tagged proteins (bottom).

(C) GFP-Trap beads were used to purify GFP-optineurin from cellular lysates of HEK293T transfected cells. Washed beads were incubated with the indicated eluted GST proteins and immunoblotting was performed using anti-GST. Ponceau staining shows comparable loading of GFP-optineurin (top).

contribution of the MIU region further, we analyzed by FP the behavior of a myosin VI iso2 construct in which the alanine at position 1,013 was mutated to glycine to abrogate MIU binding (Penengo et al., 2006). The results validated the hypothesis, as the MIU mutation did not change the iso2 affinity for K63-linked diubiquitin but reduced affinity toward K11-linked diubiquitin 6-fold (Figures 6E and S4G).

In an effort to understand why longer isoforms (iso1/3) exhibit reduced affinity for ubiquitin chains compared to the isoform with no insert (iso2), we produced a fragment that extends from the MIU region to just before the MyUb, spanning Q998–A1071 of the longer myosin VI isoform (iso3; Figure 6A). This region includes the LI, which is deleted in the short myosin VI isoform (iso2; Figure 6A). By using NMR techniques, we solved the 3D structure of the iso3 Q998–A1071 fragment, which contains the MIU domain and the LI (a snapshot is provided in Figure 6F). This analysis revealed the presence of three helices, including the anticipated MIU (Q998–E1022), a common linker helix (linker-α1, D1026–R1036), and an isoform-specific helix (linker-α2, P1055–L1066). A three-residue kink follows the MIU, while an 18-amino acid flexible region separates linker-α1 and linker-α2 (Figure 6F). Long-range NOE interactions among the three helices were not observed (data not shown). The relative configuration of MIU and linker-α1 is constrained by the short intervening region (Figures S4H and S4I), whereas linker-α1 and linker-α2 are widely distributed due to their long, flexible loop sequence (Figures S4I and S4J).

Based on these results, we hypothesized that linker-α2 is sufficient to limit MyUb:ubiquitin interaction. To test this idea, we evaluated binding to K63-linked diubiquitin of various MyUb constructs. As previously shown by a GST pull-down assay (Figure 2D), G1080–R1131 and G1080–H1122 constructs demonstrated an almost identical affinity for K63 diubiquitin (Figure S2K). By contrast, myosin VI 1050–1131, which includes linker-α2, exhibited a 4-fold reduction in binding affinity compared to the MyUb domain alone (Figure S2K). Altogether, these data led us to conclude that the isoform-specific helix linker-α2 restricts MyUb binding to ubiquitin.

DISCUSSION

Myosin VI as a Ubiquitin Receptor

We describe here a previously unanticipated structural domain in myosin VI with a helix-turn-helix-like configuration that is stabilized by a folded back N-terminal loop. This small domain, which we name MyUb, binds to ubiquitin chains, with preference for K63, K11, and K29 linkages (Figure 1D). We find that MyUb nestles between K63-linked ubiquitins and that K48 is part of a unique binding surface on the proximal ubiquitin (Figure 3C). This recognition mode provides a rationale for MyUb binding to K48-linked diubiquitin with 10-fold lower affinity compared to K63-linked diubiquitin (Figure 1E). In binding to K11-linked diubiquitin, MyUb engages the classic hydrophobic patch on the proximal ubiquitin moiety in a manner akin to its interaction with the distal ubiquitin of K63-linked chains (Figure 4). Future experiments are needed to determine how MyUb recognizes K11- and K29-linked ubiquitin chains; however, we provide evidence that the MIU plays a role in binding to K11-linked ubiquitin chains that is not recapitulated for K63-linked ubiquitin chains (Figures 6E, S4E, and S4G).

The demonstrated binding with K63-linked ubiquitin chains is consistent with the well-established role played by myosin VI in intracellular transport of endocytic vesicles (Buss et al., 2004; Tumbarello et al., 2013). Indeed, K63-linked ubiquitin chains function in cell signaling and membrane trafficking events (Acconcia et al., 2009). K63- and K11-linked ubiquitin chains may also coexist in ubiquitinated substrates, such as in the case of the major histocompatibility complex class I (MHC I), where these signals have been found to be required for efficient epsin1-dependent internalization (Boname et al., 2010; Goto et al., 2010). In this context, ubiquitin binding could contribute to the association of myosin VI with known interactors, adding an additional interaction layer of regulation. As a proof of principle, we tested optineurin, and our experiment appears to support this idea (Figure 5).

As a K11-linked ubiquitin receptor, myosin VI remains to be explored. During cell-cycle progression, the anaphase-promoting complex/cyclosome (APC/C) modifies substrates

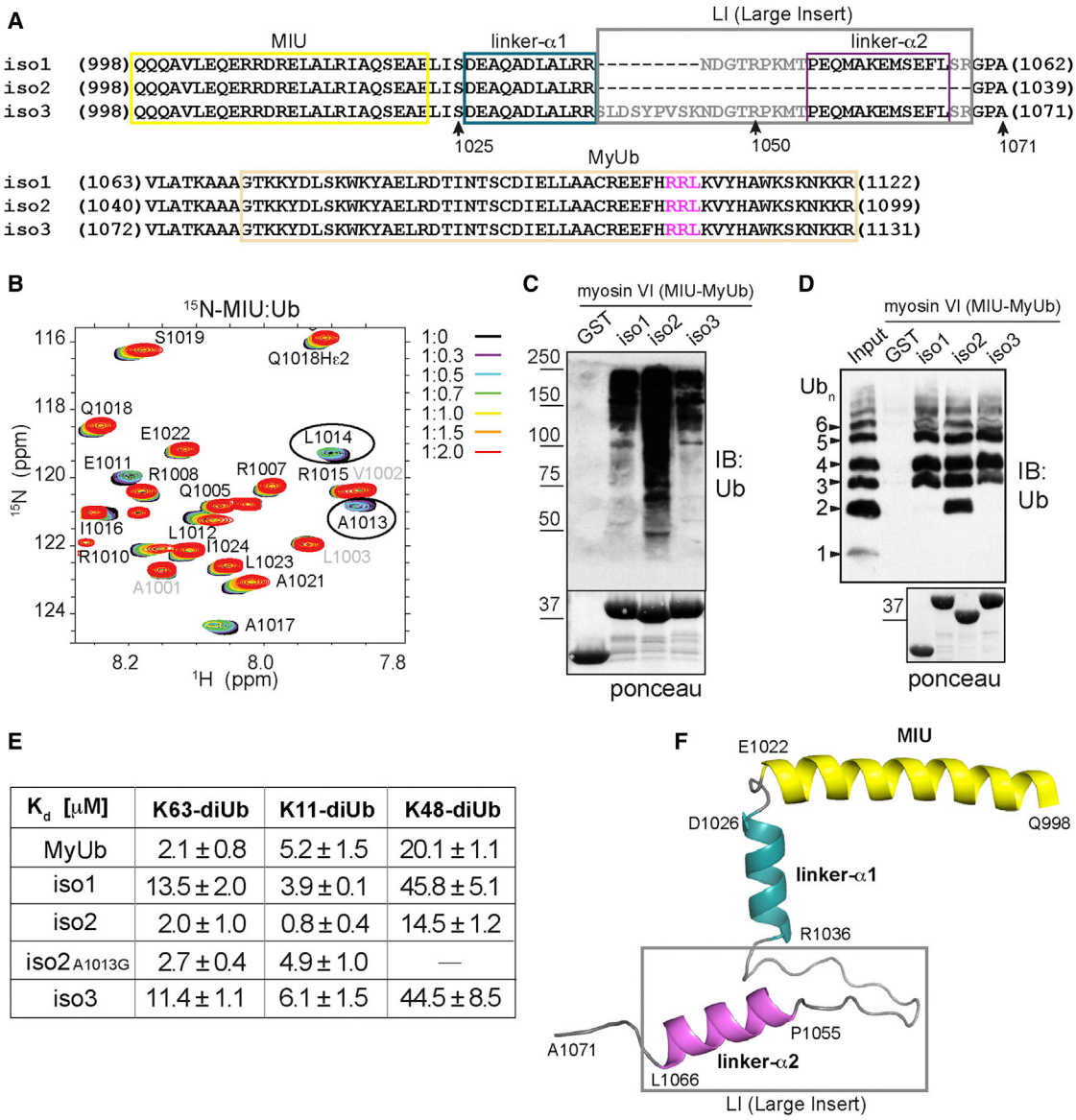

K_d [μM]	K63-diUb	K11-diUb	K48-diUb
MyUb	2.1 ± 0.8	5.2 ± 1.5	20.1 ± 1.1
iso1	13.5 ± 2.0	3.9 ± 0.1	45.8 ± 5.1
iso2	2.0 ± 1.0	0.8 ± 0.4	14.5 ± 1.2
iso2$_{A1013G}$	2.7 ± 0.4	4.9 ± 1.0	—
iso3	11.4 ± 1.1	6.1 ± 1.5	44.5 ± 8.5

Figure 6. The Presence of an Isoform-Specific Helix in the MIU-MyUb Region of Myosin VI Affects Its Affinity for Ubiquitin Chains

(A) Sequence alignment of myosin VI isoforms spanning MIU (yellow box) to MyUb (beige box). Linker-α1 (boxed in blue) and linker-α2 (boxed in purple) are indicated. The RRL motif is highlighted in magenta. Amino acids from the LI region are boxed in gray.

(B) Expanded region of ^{1}H-^{15}N HSQC spectra recorded on 0.1 mM ^{15}N MIU (Q998–S1025) with unlabeled monoubiquitin added at the indicated molar ratio. This dataset was acquired at 700 MHz.

(C) GST-tagged myosin VI MIU-MyUb constructs from the different isoforms were used to pull down polyubiquitinated proteins from HEK293T cellular lysates (1 μg). GST was used as a control, immunoblotting (IB) was done with anti-ubiquitin antibody, and Ponceau staining is included below to indicate loading of GST-tagged proteins.

(D) GST pull-down assay for 2 μM indicated myosin VI GST-MIU-MyUb or GST (as a control) with 2 hr incubation with K63-linked ubiquitin chains at 4°C. Analysis was done by immunoblotting (IB) with anti-ubiquitin antibody. All six isoforms bind longer chains, but only iso2 MIU-MyUb retains binding to K63-linked diubiquitin. Bottom: Ponceau staining showing equal loading of the GST proteins.

(E) Binding affinities (± SD) determined by FP between K63-, K11-, and K48-linked diubiquitin and the indicated myosin VI constructs.

(F) Snapshot ribbon representation of the solution structure of iso3 Q998–A1071. MIU is part of a 6.5-turn helix (yellow), which is followed by a three-residue kink and 2.5-turn helix (linker-α1, blue). A long, flexible linker region separates linker-α1 from isoform-specific linker-α2 (pink), and the orientation of these two helices is not defined. Amino acids from the LI region are boxed in gray.

See also Figure S4.

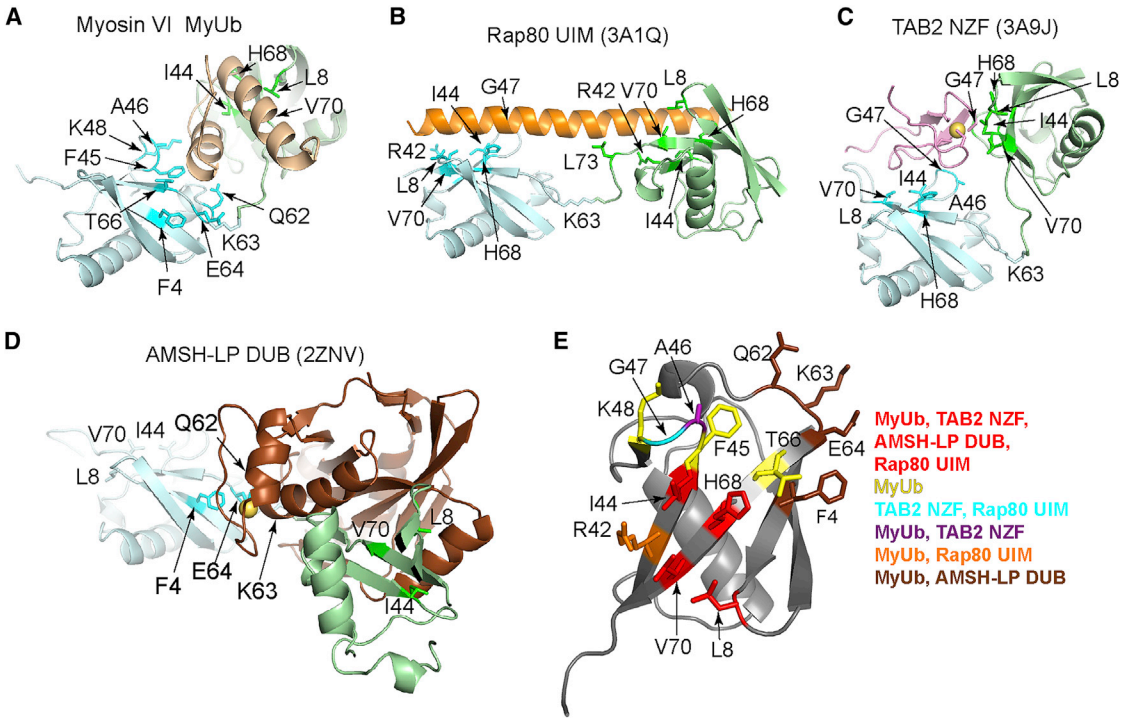

Figure 7. MyUb Interaction with K63-Linked Ubiquitin Chains Is Unique

(A–D) Structures of (A) myosin VI MyUb: K63-linked diubiquitin, (B) Rap80 UIM: K63-linked diubiquitin (3A1Q), (C) TAB2 NZF: K63-linked diubiquitin (3A9J), and (D) AMSH-LP DUB: K63-linked diubiquitin (2ZNV) displayed with their proximal ubiquitin in the same orientation. The proximal ubiquitin is depicted in light blue and the distal ubiquitin in light green. Amino acids in proximal and distal ubiquitin at the contact surface are displayed in blue and green, respectively, and labeled. (E) Structure of monomeric ubiquitin highlighting the amino acids involved in binding to K63-linked chain specific receptors, as assessed by coordinates deposited in the Protein Data Bank (PDB: 3A1Q, 3A9J, and 2ZNV) and our structure (A). A legend is included to the right illustrating the color coding with corresponding amino acids on monoubiquitin for the listed binding domains. Amino acids in yellow are unique to MyUb binding.

with ubiquitin chains linked by multiple lysines (heterotypic chains) that contain stretches of K11 linkages, allowing for their expedient degradation by the proteasome (Meyer and Rape, 2014). A recent study suggests that the need for heterotypic chains may be derived from poor binding to mammalian proteasome of ubiquitin chains that are linked exclusively by K11 (Grice et al., 2015). Notably, a few reports suggest a nuclear function for myosin VI (Vreugde et al., 2006; Zorca et al., 2015). In this subcellular compartment, myosin VI may interact with proteins modified by K11-linked chains to regulate transcription and viral infection.

MyUb Binding to K63-Linked Ubiquitin Chains

Our structural results indicate that the MyUb nestles between the neighboring moieties of a K63-linked diubiquitin, making extensive contacts around the ubiquitin ligation site (Figures 3C, 3G, and 7A). We compared our MyUb:K63-linked diubiquitin structure to other solved structures of ubiquitin receptors in complex with K63-linked ubiquitin chains. All of them make direct interaction with ubiquitin at positions L8, I44, H68, and V70 (Figures 7B–7D). Rap80 uses two UIMs that are registered in a contiguous helix to bind neighboring ubiquitins of K63-linked ubiquitin chains (Sims and Cohen, 2009) (Figure 7B). A small compact TAB2 NZF domain uses two distinct surfaces to bind the I44-centered surface of both ubiquitins in K63-linked ubiquitin chains (Kulathu et al., 2009; Sato et al., 2009) (Figure 7C) in a binding mode similar to hHR23A UBA2 domain binding to K48-linked ubiquitin chains (Varadan et al., 2005). Deubiquitinase AMSH-LP forms direct interactions with the K63 linker region to achieve linkage specificity engaging K63 and surrounding Q62, E64, and F4 (Sato et al., 2008) (Figure 7D). In contrast to the above-mentioned domains, MyUb binds to K63-linked ubiquitin chains by engaging the canonical hydrophobic surface on distal ubiquitin and a unique surface on proximal ubiquitin that includes F45, K48, N60, Q62, and T66 (Figures 7A and 7D).

Finally, it is important to appraise the MyUb in the context of the myosin VI protein. Our study established that the binding of MyUb to ubiquitin is regulated by two other nearby structural elements. The first one is the MIU, which shows limited ubiquitin-binding ability by itself (Figures 1E and 6B) and does not appear to contribute to the overall binding of myosin VI to K63-linked diubiquitin but does participate in its binding to K11-linked diubiquitin (Figure 6E). These data suggest that myosin VI domains evolved in order to recognize and accommodate specific diubiquitin signals. The second element of regulation is the isoform-specific helix linker-α2, which is capable of modulating myosin VI interaction with ubiquitin, as iso1 and iso3 showed reduced binding compared to iso2 for all diubiquitin chain types tested (Figure 6E). This region could potentially regulate isoform-specific myosin VI functions. For a thorough understanding of

these elements and their functions, additional structural and functional studies are needed.

Implications for RRL Interactors

Embedded in the MyUb is the RRL motif previously identified as critical for interaction with endocytic and autophagic adaptors (Tumbarello et al., 2013). We demonstrate here that R1117 from this motif is crucial for MyUb structure integrity. Our findings underline the requirement of an extended hydrophobic surface on Helix2 of the MyUb (H1122–R1131) for binding to the functional adaptors optineurin, GIPC, T6BP, and NDP52 (Figures 2D and 2E). In addition, we showed that optineurin may undergo ubiquitination and that I1104 on MyUb is critical for myosin VI binding to this autophagic adaptor (Figure 5). Although we cannot formally exclude the possibility that I1104 is part of the direct binding site, our data suggest that MyUb binding to ubiquitin on optineurin may regulate the interaction between myosin VI and optineurin in space and time, a hypothesis that is consistent with previous literature (Liu et al., 2014). This additional layer of regulation can be particularly relevant in the context of selective autophagy, where both proteins were recently implicated (Tumbarello et al., 2012, 2015), or in cell migration for which we have demonstrated a critical role exerted by iso2 myosin VI and optineurin (Wollscheid et al., 2016).

Altogether, the fundamental insights we have generated within this study provide the basis for future studies that interrogate how myosin VI interacts with functional adaptors for downstream signaling.

EXPERIMENTAL PROCEDURES

Reagents, Antibodies, Protein Expression and Purification, and Cell Lines

Information regarding reagents, including the production of protein samples, antibodies, and cell culturing can be found in Supplemental Experimental Procedures. GFP-optineurin, FLAG-T6BP, His-GIPC, and FLAG-NDP52 were generously provided by Dr. Alain Israel, Dr. Folma Buss, Dr. Guido Serini, and Dr. Felix Randow, respectively. Hemagglutinin (HA)-ubiquitin was previously described (Polo et al., 2002).

Size Exclusion Chromatography

100 μM K63-linked diubiquitin or triubiquitin was incubated at different molar ratios with MyUb (G1080–R1131) for 1 hr at 20°C and subjected to size exclusion chromatography on a Superdex75 (5/150) column using the ÄKTA microsystem (GE Healthcare). Fractions containing complex or single proteins were analyzed by SDS-PAGE and Coomassie staining.

Fluorescence Polarization Assay

The thiol-reactive fluorescent probe BODIPY TMR C5-maleimide (Invitrogen) was conjugated to diubiquitin G76C linked via K11, K48, or K63 (100 μM, in 20 mM Tris-HCl [pH 7.6], 200 mM NaCl, 5% glycerol, and 1 mM tris(2-carboxyethyl)phosphine [TCEP]) following the manufacturer's instructions. Briefly, a 20 mM stock solution of lyophilized dye suspended in DMSO was diluted into the protein solution at 10-fold molar excess and the conjugation reaction allowed to proceed for 2 hr in the dark at 4°C. The reaction mixture was dialyzed against 20 mM Tris-HCl [pH 7.6], 200 mM NaCl, and 5% glycerol to remove excess dye and then loaded on a Superdex75 10/300 column (GE Healthcare) to isolate labeled proteins, monitored by absorbance at 544 nm. Fluorescence polarization assays were performed at 22°C with $\lambda_{excitation}$ at 535 nm and $\lambda_{emission}$ at 580 nm on a 384-well plate by using an Infinite 200 instrument (Tecan). Concentrations in the nanomolar range (20–50 nM) of labeled proteins were titrated with MyUb (280–300 μM). Polarization readings from three independent replicates were averaged and fitted as previously described (Eletr et al., 2005). Experiments were repeated at least three times, and the reported K_d values represent the mean ± SD.

GST Pull-Down Experiments

Detailed procedures used for GST pull-down experiments can be found in Supplemental Experimental Procedures.

NMR Spectroscopy and Structure Determination

Detailed procedures for collecting and analyzing NMR data as well as for calculating, evaluating, and presenting the protein structures can be found in Supplemental Experimental Procedures.

ACCESSION NUMBERS

The accession numbers for the structural coordinates and chemical shift data for MyUb (G1080–H1122), MyUb (G1080–R1131), iso3 Q998–A1071, and MyUb (G1080–H1122):K63-linked diubiquitin are PDB: 2N0Z and BMRB: 25541, PDB: 2N10 and BMRB: 25542, PDB: 2N11 and BMRB: 25543, and PDB: 2N13 and BMRB: 25545, respectively.

SUPPLEMENTAL INFORMATION

Supplemental Information includes Supplemental Experimental Procedures, four figures, and one table and can be found with this article online at http://dx.doi.org/10.1016/j.celrep.2016.01.079.

AUTHOR CONTRIBUTIONS

F.H. performed, analyzed, and interpreted all NMR experiments with the exception of backbone assignments for MyUb (G1080–R1131), which was done with assistance from A.E.; H.-P.W. biochemically characterized the MyUb domain and its selective interaction with ubiquitin and adaptor proteins with the help of M.B.; E.V. carried out all FP analyses; U.N. helped F.H. with NMR titration experiments and generating ubiquitin species for FP experiments; F.A. initially identified the MyUb domain; E.M. performed the experiment shown in Figure 5; S.P. and K.J.W. conceived of and directed the project; and all authors contributed to manuscript writing.

ACKNOWLEDGMENTS

This research was funded by the Intramural Research Program of the NIH, Center for Cancer Research (to K.J.W.); by a grant from the NIH (CA136472) (to K.J.W.); by the Association for International Cancer Research (AICR, grant 11-0051) (to S.P.); and by the Italian Ministry of Education, Universities and Research (PRIN 20108MXN2J) (to S.P.). We are grateful to Dr. Janusz Koscielniak for his technical assistance with the NMR facility.

Received: June 10, 2015
Revised: November 24, 2015
Accepted: January 27, 2016
Published: March 10, 2016

REFERENCES

Acconcia, F., Sigismund, S., and Polo, S. (2009). Ubiquitin in trafficking: the network at work. Exp. Cell Res. *315*, 1610–1618.

Au, J.S., Puri, C., Ihrke, G., Kendrick-Jones, J., and Buss, F. (2007). Myosin VI is required for sorting of AP-1B-dependent cargo to the basolateral domain in polarized MDCK cells. J. Cell Biol. *177*, 103–114.

Avraham, K.B., Hasson, T., Steel, K.P., Kingsley, D.M., Russell, L.B., Moosekker, M.S., Copeland, N.G., and Jenkins, N.A. (1995). The mouse Snell's waltzer deafness gene encodes an unconventional myosin required for structural integrity of inner ear hair cells. Nat. Genet. *11*, 369–375.

Berg, J.S., Powell, B.C., and Cheney, R.E. (2001). A millennial myosin census. Mol. Biol. Cell *12*, 780–794.

Boname, J.M., Thomas, M., Stagg, H.R., Xu, P., Peng, J., and Lehner, P.J. (2010). Efficient internalization of MHC I requires lysine-11 and lysine-63 mixed linkage polyubiquitin chains. Traffic *11*, 210–220.

Bond, L.M., Tumbarello, D.A., Kendrick-Jones, J., and Buss, F. (2013). Small-molecule inhibitors of myosin proteins. Future Med. Chem. *5*, 41–52.

Bunn, R.C., Jensen, M.A., and Reed, B.C. (1999). Protein interactions with the glucose transporter binding protein GLUT1CBP that provide a link between GLUT1 and the cytoskeleton. Mol. Biol. Cell *10*, 819–832.

Buss, F., Arden, S.D., Lindsay, M., Luzio, J.P., and Kendrick-Jones, J. (2001). Myosin VI isoform localized to clathrin-coated vesicles with a role in clathrin-mediated endocytosis. EMBO J. *20*, 3676–3684.

Buss, F., Spudich, G., and Kendrick-Jones, J. (2004). Myosin VI: cellular functions and motor properties. Annu. Rev. Cell Dev. Biol. *20*, 649–676.

Chibalina, M.V., Seaman, M.N., Miller, C.C., Kendrick-Jones, J., and Buss, F. (2007). Myosin VI and its interacting protein LMTK2 regulate tubule formation and transport to the endocytic recycling compartment. J. Cell Sci. *120*, 4278–4288.

Dunn, T.A., Chen, S., Faith, D.A., Hicks, J.L., Platz, E.A., Chen, Y., Ewing, C.M., Sauvageot, J., Isaacs, W.B., De Marzo, A.M., and Luo, J. (2006). A novel role of myosin VI in human prostate cancer. Am. J. Pathol. *169*, 1843–1854.

Ehlinger, A., and Walters, K.J. (2013). Structural insights into proteasome activation by the 19S regulatory particle. Biochemistry *52*, 3618–3628.

Eletr, Z.M., Huang, D.T., Duda, D.M., Schulman, B.A., and Kuhlman, B. (2005). E2 conjugating enzymes must disengage from their E1 enzymes before E3-dependent ubiquitin and ubiquitin-like transfer. Nat. Struct. Mol. Biol. *12*, 933–934.

Finan, D., Hartman, M.A., and Spudich, J.A. (2011). Proteomics approach to study the functions of Drosophila myosin VI through identification of multiple cargo-binding proteins. Proc. Natl. Acad. Sci. USA *108*, 5566–5571.

Geeves, M.A., and Holmes, K.C. (1999). Structural mechanism of muscle contraction. Annu. Rev. Biochem. *68*, 687–728.

Gibson, F., Walsh, J., Mburu, P., Varela, A., Brown, K.A., Antonio, M., Beisel, K.W., Steel, K.P., and Brown, S.D. (1995). A type VII myosin encoded by the mouse deafness gene shaker-1. Nature *374*, 62–64.

Goto, E., Yamanaka, Y., Ishikawa, A., Aoki-Kawasumi, M., Mito-Yoshida, M., Ohmura-Hoshino, M., Matsuki, Y., Kajikawa, M., Hirano, H., and Ishido, S. (2010). Contribution of lysine 11-linked ubiquitination to MIR2-mediated major histocompatibility complex class I internalization. J. Biol. Chem. *285*, 35311–35319.

Grice, G.L., Lobb, I.T., Weekes, M.P., Gygi, S.P., Antrobus, R., and Nathan, J.A. (2015). The Proteasome Distinguishes between Heterotypic and Homotypic Lysine-11-Linked Polyubiquitin Chains. Cell Rep. *12*, 545–553.

Hasson, T., Heintzelman, M.B., Santos-Sacchi, J., Corey, D.P., and Mooseker, M.S. (1995). Expression in cochlea and retina of myosin VIIa, the gene product defective in Usher syndrome type 1B. Proc. Natl. Acad. Sci. USA *92*, 9815–9819.

Inoue, A., Sato, O., Homma, K., and Ikebe, M. (2002). DOC-2/DAB2 is the binding partner of myosin VI. Biochem. Biophys. Res. Commun. *292*, 300–307.

Kulathu, Y., Akutsu, M., Bremm, A., Hofmann, K., and Komander, D. (2009). Two-sided ubiquitin binding explains specificity of the TAB2 NZF domain. Nat. Struct. Mol. Biol. *16*, 1328–1330.

Kumar, M., Sackey, K., Schmalstieg, F., Trizna, Z., Elghetany, M.T., and Alter, B.P. (2001). Griscelli syndrome: rare neonatal syndrome of recurrent hemophagocytosis. J. Pediatr. Hematol. Oncol. *23*, 464–468.

Liu, F., and Walters, K.J. (2010). Multitasking with ubiquitin through multivalent interactions. Trends Biochem. Sci. *35*, 352–360.

Liu, Z., Chen, P., Gao, H., Gu, Y., Yang, J., Peng, H., Xu, X., Wang, H., Yang, M., Liu, X., et al. (2014). Ubiquitylation of autophagy receptor Optineurin by HACE1 activates selective autophagy for tumor suppression. Cancer Cell *26*, 106–120.

Ménétrey, J., Bahloul, A., Wells, A.L., Yengo, C.M., Morris, C.A., Sweeney, H.L., and Houdusse, A. (2005). The structure of the myosin VI motor reveals the mechanism of directionality reversal. Nature *435*, 779–785.

Meyer, H.J., and Rape, M. (2014). Enhanced protein degradation by branched ubiquitin chains. Cell *157*, 910–921.

Mohiddin, S.A., Ahmed, Z.M., Griffith, A.J., Tripodi, D., Friedman, T.B., Fananapazir, L., and Morell, R.J. (2004). Novel association of hypertrophic cardiomyopathy, sensorineural deafness, and a mutation in unconventional myosin VI (MYO6). J. Med. Genet. *41*, 309–314.

Morris, S.M., Arden, S.D., Roberts, R.C., Kendrick-Jones, J., Cooper, J.A., Luzio, J.P., and Buss, F. (2002). Myosin VI binds to and localises with Dab2, potentially linking receptor-mediated endocytosis and the actin cytoskeleton. Traffic *3*, 331–341.

Morriswood, B., Ryzhakov, G., Puri, C., Arden, S.D., Roberts, R., Dendrou, C., Kendrick-Jones, J., and Buss, F. (2007). T6BP and NDP52 are myosin VI binding partners with potential roles in cytokine signalling and cell adhesion. J. Cell Sci. *120*, 2574–2585.

Penengo, L., Mapelli, M., Murachelli, A.G., Confalonieri, S., Magri, L., Musacchio, A., Di Fiore, P.P., Polo, S., and Schneider, T.R. (2006). Crystal structure of the ubiquitin binding domains of rabex-5 reveals two modes of interaction with ubiquitin. Cell *124*, 1183–1195.

Polo, S., Sigismund, S., Faretta, M., Guidi, M., Capua, M.R., Bossi, G., Chen, H., De Camilli, P., and Di Fiore, P.P. (2002). A single motif responsible for ubiquitin recognition and monoubiquitination in endocytic proteins. Nature *416*, 451–455.

Sahlender, D.A., Roberts, R.C., Arden, S.D., Spudich, G., Taylor, M.J., Luzio, J.P., Kendrick-Jones, J., and Buss, F. (2005). Optineurin links myosin VI to the Golgi complex and is involved in Golgi organization and exocytosis. J. Cell Biol. *169*, 285–295.

Sato, Y., Yoshikawa, A., Yamagata, A., Mimura, H., Yamashita, M., Ookata, K., Nureki, O., Iwai, K., Komada, M., and Fukai, S. (2008). Structural basis for specific cleavage of Lys 63-linked polyubiquitin chains. Nature *455*, 358–362.

Sato, Y., Yoshikawa, A., Yamashita, M., Yamagata, A., and Fukai, S. (2009). Structural basis for specific recognition of Lys 63-linked polyubiquitin chains by NZF domains of TAB2 and TAB3. EMBO J. *28*, 3903–3909.

Sellers, J.R. (2000). Myosins: a diverse superfamily. Biochim. Biophys. Acta *1496*, 3–22.

Shen, W.C., Li, H.Y., Chen, G.C., Chern, Y., and Tu, P.H. (2015). Mutations in the ubiquitin-binding domain of OPTN/optineurin interfere with autophagy-mediated degradation of misfolded proteins by a dominant-negative mechanism. Autophagy *11*, 685–700.

Sims, J.J., and Cohen, R.E. (2009). Linkage-specific avidity defines the lysine 63-linked polyubiquitin-binding preference of rap80. Mol. Cell *33*, 775–783.

Spudich, J.A., and Sivaramakrishnan, S. (2010). Myosin VI: an innovative motor that challenged the swinging lever arm hypothesis. Nat. Rev. Mol. Cell Biol. *11*, 128–137.

Spudich, G., Chibalina, M.V., Au, J.S., Arden, S.D., Buss, F., and Kendrick-Jones, J. (2007). Myosin VI targeting to clathrin-coated structures and dimerization is mediated by binding to Disabled-2 and PtdIns(4,5)P2. Nat. Cell Biol. *9*, 176–183.

Takagishi, Y., and Murata, Y. (2006). Myosin Va mutation in rats is an animal model for the human hereditary neurological disease, Griscelli syndrome type 1. Ann. N Y Acad. Sci. *1086*, 66–80.

Tomatis, V.M., Papadopulos, A., Malintan, N.T., Martin, S., Wallis, T., Gormal, R.S., Kendrick-Jones, J., Buss, F., and Meunier, F.A. (2013). Myosin VI small insert isoform maintains exocytosis by tethering secretory granules to the cortical actin. J. Cell Biol. *200*, 301–320.

Tumbarello, D.A., Waxse, B.J., Arden, S.D., Bright, N.A., Kendrick-Jones, J., and Buss, F. (2012). Autophagy receptors link myosin VI to autophagosomes to mediate Tom1-dependent autophagosome maturation and fusion with the lysosome. Nat. Cell Biol. *14*, 1024–1035.

Tumbarello, D.A., Kendrick-Jones, J., and Buss, F. (2013). Myosin VI and its cargo adaptors - linking endocytosis and autophagy. J. Cell Sci. *126*, 2561–2570.

Tumbarello, D.A., Manna, P.T., Allen, M., Bycroft, M., Arden, S.D., Kendrick-Jones, J., and Buss, F. (2015). The Autophagy Receptor TAX1BP1 and the Molecular Motor Myosin VI Are Required for Clearance of Salmonella Typhimurium by Autophagy. PLoS Pathog. *11*, e1005174.

Varadan, R., Assfalg, M., Raasi, S., Pickart, C., and Fushman, D. (2005). Structural determinants for selective recognition of a Lys48-linked polyubiquitin chain by a UBA domain. Mol. Cell *18*, 687–698.

Vreugde, S., Ferrai, C., Miluzio, A., Hauben, E., Marchisio, P.C., Crippa, M.P., Bussi, M., and Biffo, S. (2006). Nuclear myosin VI enhances RNA polymerase II-dependent transcription. Mol. Cell *23*, 749–755.

Walters, K.J., Ferentz, A.E., Hare, B.J., Hidalgo, P., Jasanoff, A., Matsuo, H., and Wagner, G. (2001). Characterizing protein-protein complexes and oligomers by nuclear magnetic resonance spectroscopy. Methods Enzymol. *339*, 238–258.

Weil, D., Blanchard, S., Kaplan, J., Guilford, P., Gibson, F., Walsh, J., Mburu, P., Varela, A., Levilliers, J., Weston, M.D., et al. (1995). Defective myosin VIIA gene responsible for Usher syndrome type 1B. Nature *374*, 60–61.

Wells, A.L., Lin, A.W., Chen, L.Q., Safer, D., Cain, S.M., Hasson, T., Carragher, B.O., Milligan, R.A., and Sweeney, H.L. (1999). Myosin VI is an actin-based motor that moves backwards. Nature *401*, 505–508.

Wollscheid, H.-P., Biancospino, M., He, F., Magistrati, E., Molteni, E., Lupia, M., Soffientini, P., Rottner, K., Cavallaro, U., Pozzoli, U., et al. (2016). Diverse functions of myosin VI elucidated by an isoform-specific α-helix domain. Nat. Struct. Mol. Biol. http://dx.doi.org/10.1038/nsmb.3187

Yoshida, H., Cheng, W., Hung, J., Montell, D., Geisbrecht, E., Rosen, D., Liu, J., and Naora, H. (2004). Lessons from border cell migration in the Drosophila ovary: A role for myosin VI in dissemination of human ovarian cancer. Proc. Natl. Acad. Sci. USA *101*, 8144–8149.

Zorca, C.E., Kim, L.K., Kim, Y.J., Krause, M.R., Zenklusen, D., Spilianakis, C.G., and Flavell, R.A. (2015). Myosin VI regulates gene pairing and transcriptional pause release in T cells. Proc. Natl. Acad. Sci. USA *112*, E1587–E1593.